

Prostate tumor–derived GDF11 accelerates androgen deprivation therapy–induced sarcopenia

Chunliu Pan,¹ Neha Jaiswal Agrawal,¹ Yanni Zulia,¹ Shalini Singh,¹ Kai Sha,¹ James L. Mohler,² Kevin H. Eng,^{1,3} Joe V. Chakkalakal,^{4,5} John J. Krolewski,¹ and Kent L. Nastiuk^{1,2}

¹Department of Cancer Genetics and Genomics, ²Department of Urology, and ³Department of Biostatistics and Bioinformatics, Roswell Park Comprehensive Cancer Center, Buffalo, New York, USA. ⁴Department of Pharmacology & Physiology and ⁵Department of Biomedical Engineering, University of Rochester Medical Center, Rochester, New York, USA.

Most prostate cancers depend on androgens for growth, and therefore, the mainstay treatment for advanced, recurrent, or metastatic prostate cancer is androgen deprivation therapy (ADT). A prominent side effect in patients receiving ADT is an obese frailty syndrome that includes fat gain and sarcopenia, defined as the loss of muscle function accompanied by reduced muscle mass or quality. Mice bearing Pten-deficient prostate cancers were examined to gain mechanistic insight into ADT-induced sarcopenic obesity. Castration induced fat gain as well as skeletal muscle mass and strength loss. Catabolic TGF- β family myokine protein levels were increased immediately prior to strength loss, and pan-myokine blockade using a soluble receptor (ActRIIB-Fc) completely reversed the castration-induced sarcopenia. The onset of castration-induced strength and muscle mass loss, as well as the increase in catabolic TGF- β family myokine protein levels, were coordinately accelerated in tumor-bearing mice relative to tumor-free mice. Notably, growth differentiation factor 11 (GDF11) increased in muscle after castration only in tumor-bearing mice, but not in tumor-free mice. An early surge of GDF11 in prostate tumor tissue and in the circulation suggests that endocrine GDF11 signaling from tumor to muscle is a major driver of the accelerated ADT-induced sarcopenic phenotype. In tumor-bearing mice, GDF11 blockade largely prevented castration-induced strength loss but did not preserve muscle mass, which confirms a primary role for GDF11 in muscle function and suggests an additional role for the other catabolic myokines.

Introduction

While many men diagnosed with prostate cancer (PrCa) are cured with local therapy, the principal treatment for PrCa control in patients who present with more advanced disease, are medically unfit for local therapy, or have recurrent PrCa is androgen deprivation therapy (ADT) (1). ADT, whether surgical or drug induced, reduces serum testosterone to castrate levels (2) and causes tumor cell apoptosis (3). Men may be on continuous ADT, often with additional second-line androgen signaling suppression, for 10 or more years (4). Some ADT-induced side effects (erectile dysfunction, osteopenia, depression) can be managed medically, but other side effects (cognitive changes, metabolic dysregulation, sarcopenia) need more effective interventions (5). Sarcopenia is the loss of muscle function, defined by strength, power, or physical performance, due to low muscle mass or muscle quality (6). ADT-induced sarcopenia is accompanied by fat gain, and both increase with the duration of ADT (7). Adiposity increases fat infiltration into muscle, thereby reducing muscle quality and further degrading muscle function (8, 9). The loss of muscle mass but not fat mass differentiates ADT-induced sarcopenia from tumor cachexia, which is marked by loss of mass in both compartments (10). Despite frequent overall weight gain resulting from adiposity in men receiving ADT, these men lose strength, resulting in functional deficits, including an increased risk of falls and fractures (11). Thus, ADT-induced sarcopenia is most likely the underlying mechanism accounting for an “obese frailty” syndrome described in men receiving ADT for PrCa (12). A combination of exercise and testosterone therapy can reverse frailty in many populations, but these interventions are problematic for many patients with PrCa (13–15).

We previously reported that ADT-induced sarcopenia in normal (tumor-free) mice closely resembles the obese frailty phenotype seen in patients (16). Specifically, tumor-free mice exhibited loss of skeletal

Authorship note: CP and NJA contributed equally to this work.

Conflict of interest: The authors have declared that no conflict of interest exists.

Copyright: © 2020, American Society for Clinical Investigation.

Submitted: December 21, 2018

Accepted: February 19, 2020

Published: February 20, 2020.

Reference information: *JCI Insight*. 2020;5(6):e127018.

<https://doi.org/10.1172/jci.insight.127018>.

muscle strength, reduced lean muscle mass, and increased adipose tissue. Castration specifically reduced muscle cross-sectional area and muscle absolute force production (17). Sarcopenia onset occurred 6 weeks after castration, and myostatin and activins were induced in muscles of adult male mice before the onset of strength loss (16). Five catabolic TGF- β family myokines, including myostatin, growth differentiation factor 11 (GDF11), and the activins (homodimers composed of activin A or B and the heterodimer activin AB), are secreted by muscle and reduce muscle mass (18–20). These myokines are synthesized as inactive proproteins, which must be cleaved, covalently dimerized, and released from inhibitory proteins to become active ligands (18, 21). Catabolic TGF- β family myokines regulate muscle homeostasis via the activin type II receptors (19). A TGF- β family myokine ligand trap, ActRIIB-Fc, blocks catabolic signaling (22). ActRIIB-Fc treatment of castrated adult mice blocked sarcopenia and fat gain (16). Unfortunately, during clinical trials, ActRIIB-Fc induced vascular adverse events, including telangiectasias and mucocutaneous bleeding, likely due to off-target bone morphogenetic protein 9 (BMP9) signaling blockade (23–25). Better understanding of the mechanism of ADT-induced obese frailty in the context of PrCa may enable development of more selective therapies to preserve muscle mass and strength (26, 27).

We therefore examined ADT-induced sarcopenia in the PB-Cre4 *Pten*^{fl/fl} mouse, an autochthonous model of PrCa. Tumorigenesis in this model is driven by *Pten* loss in prostate epithelia. PTEN loss is one of the most frequent genetic lesions in localized and metastatic human PrCa (28), and it predicts patient outcomes (29), confirming its biological relevance. Like human PrCa, *Pten*-deficient murine prostate tumors grow slowly and regress after castration (30), making PB-Cre4 *Pten*^{fl/fl} mice an excellent model for investigating the side effects of ADT in patients.

In PB-Cre4 *Pten*^{fl/fl} mice bearing prostate tumors, the onset of strength loss after castration was accelerated in tumor-bearing mice relative to tumor-free mice. Analysis of catabolic myokine production in muscle, tumor, and serum as well as treatment of castrated mice with GDF11-specific blockade demonstrated that the earlier onset of the sarcopenic phenotype is driven primarily by tumor-derived GDF11 acting via an endocrine mechanism. We discuss a model for tumor-muscle interactions as well as the impact of our findings on the future development of medical therapies for ADT-induced sarcopenia in patients with PrCa.

Results

Castration induces a sarcopenia phenotype in a PrCa mouse model resembling the ADT-induced obese frailty syndrome in PrCa patients. We previously observed castration-induced sarcopenia in adult (6–9 months old) tumor-free mice that had not been detected in younger mice (16). To test the relevance of the PB-Cre4 *Pten*^{fl/fl} PrCa model, we first tested whether tumor burden alone induced sarcopenia. We monitored prostate tumor development using high-resolution high-frequency ultrasound (HFUS) imaging (Supplemental Figure 1; supplemental material available online with this article; <https://doi.org/10.1172/jci.insight.127018DS1>) and found that neither total body mass nor grip strength varied among mice bearing tumors that ranged from 514 to 4515 mm³ (Supplemental Figure 2, A and B). The mass of the skeletal muscles varied little, whether from tumor-bearing or tumor-free mice (Supplemental Figure 2C). We next determined whether castration of adult prostate tumor-bearing mice recapitulated the obese frailty phenotype seen in patients and tumor-free mice following castration. Tumor volume and grip strength were measured weekly for 16 weeks after castration (Figure 1). Castration caused tumor regression (Figure 1A), in accordance with earlier reports (30–32). Grip strength declined starting 4 weeks after castration (Figure 1B). Sixteen weeks after castration, the mass of 5 of the 6 skeletal muscles was reduced (Figure 1C), and adiposity was increased (Figure 1D). In this autochthonous PrCa model, castration of mice bearing tumors of widely varying size induced sarcopenia and fat gain, resembling the obese frailty syndrome in PrCa patients receiving ADT (12).

Cancer frequently results in cachexia, a distinct physiological entity of generalized wasting that includes both abundant lipolysis and sarcopenia, leading to lower total body mass. However, ADT-induced sarcopenia is not a consequence of cancer cachexia because castrated mice gained fat without loss of body mass. The mice used in Figure 1 had tumors of widely varying size. Larger tumors regressed more in response to castration than smaller tumors (Supplemental Figure 3A), but tumor size did not affect either castration-induced strength loss or total body mass (Supplemental Figure 3, B and C). However, mice bearing larger tumors had increased lean body mass (Supplemental Figure 3D). Neither adiposity nor the mass of isolated skeletal muscles correlated with tumor volume 16 weeks after castration (Supplemental Figure 3, E and F). We restricted future experiments to mice bearing

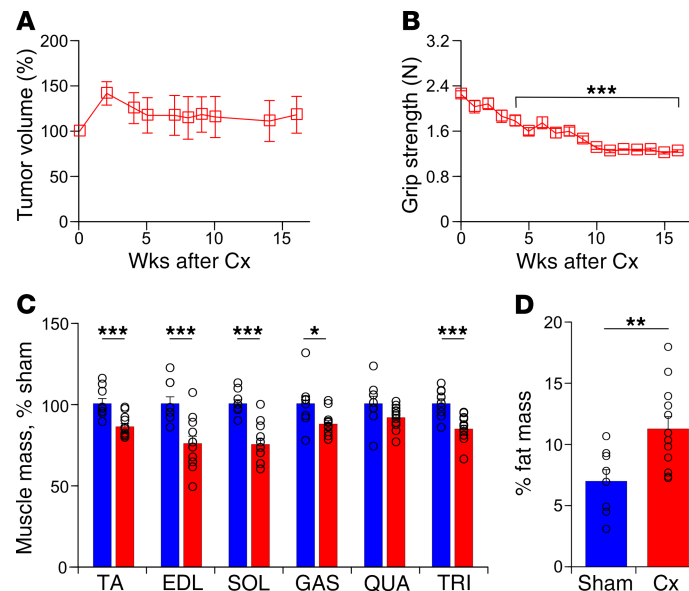


Figure 1. Castration induced strength and muscle loss as well as fat gain in tumor-bearing mice. (A) Tumor volume in adult PB-Cre4 *Pten^{fl/fl}* mice before (starting tumor volume 514–4515 mm³) and after castration (Cx), as percentage of pre-Cx volume. (B) Grip strength before and after castration, in newtons. (C) Mass of dissected skeletal muscles: tibialis anterior (TA), extensor digitorum longus (EDL), soleus (SOL), gastrocnemius (GAS), quadriceps (QUA), and triceps (TRI), 16 weeks after castration (shown in red) as percentage of sham-castrated tumor-bearing mice (shown in blue). (D) Whole-body fat mass, as a percentage of total body mass, 16 weeks after castration (red) versus sham-castrated tumor-bearing mice (blue). Mean shown as lines or columns, SEM as bars; *n* = 4 (noncastrated), 12 (castrated), indicated by open circles. **P* < 0.05; ***P* < 0.01; and ****P* < 0.001 versus pre- or sham-castrated mice determined using 1-way ANOVA with Dunnett's test (A–C) and Student's *t* test (D).

smaller, more uniform tumors because both tumor regression and lean body mass measurements were confounded by tumor size variability.

TGF-β family myokine protein levels increase prior to the onset of castration-induced sarcopenia. We next examined the effect of castration on sarcopenia and catabolic TGF-β family myokine expression in groups of adult mice that were sacrificed at 2-week intervals. Tumor volume, monitored using HFUS imaging, declined after castration (Supplemental Figure 4). Functionally, grip strength declined 3 weeks after castration (Figure 2A), similar to the timing observed in Figure 1B. Castration reduced the mass of 4 skeletal muscles (tibialis anterior, extensor digitorum longus, soleus, triceps) by 4 weeks after castration, coincident with strength loss (Figure 2B). However, mass loss was not evident until 6 weeks after castration in 2 of the larger muscles (quadriceps, gastrocnemius). Figure 3 shows the time course of catabolic TGF-β family myokine levels in 2 muscles from the mice examined in Figure 2. The levels of 4 (myostatin, GDF11, activin A, and activin B) of the 5 myokines were increased 2 weeks after castration, before the onset of strength loss, in both gastrocnemius muscle (GAS, Figure 3, A–F) and triceps muscle (TRI, Figure 3, G–L). Castration-induced changes of activin A and activin B protein levels were similar to changes observed in tumor-free mice after castration (16). However, for GDF11 there was a marked difference. Specifically, GDF11 levels were increased prior to strength loss, 2 weeks after castration in both GAS and TRI muscles of tumor-bearing mice (Figure 3, F and L), whereas in our prior report castration did not change GDF11 levels in GAS or TRI muscles before strength loss in tumor-free mice (16). We previously demonstrated that myostatin levels were increased 4 weeks after castration in tumor-free mice, before strength loss at 6 weeks (16). Myostatin levels in tumor-bearing mice were increased by 2 weeks, still before strength loss at 3 weeks after castration (Figure 2A). Myostatin showed a second, more pronounced maxima at 6 and 8 weeks after castration in the muscles of tumor-bearing mice, beyond the onset of strength loss. None of the mRNAs encoding the TGF-β family myokines or their receptors were regulated in quadriceps muscle after castration (Supplemental Figure 6), which is consistent with previously described posttranscriptional regulation of myokine proteins by proteolytic cleavage of the latent precursor (18, 33).

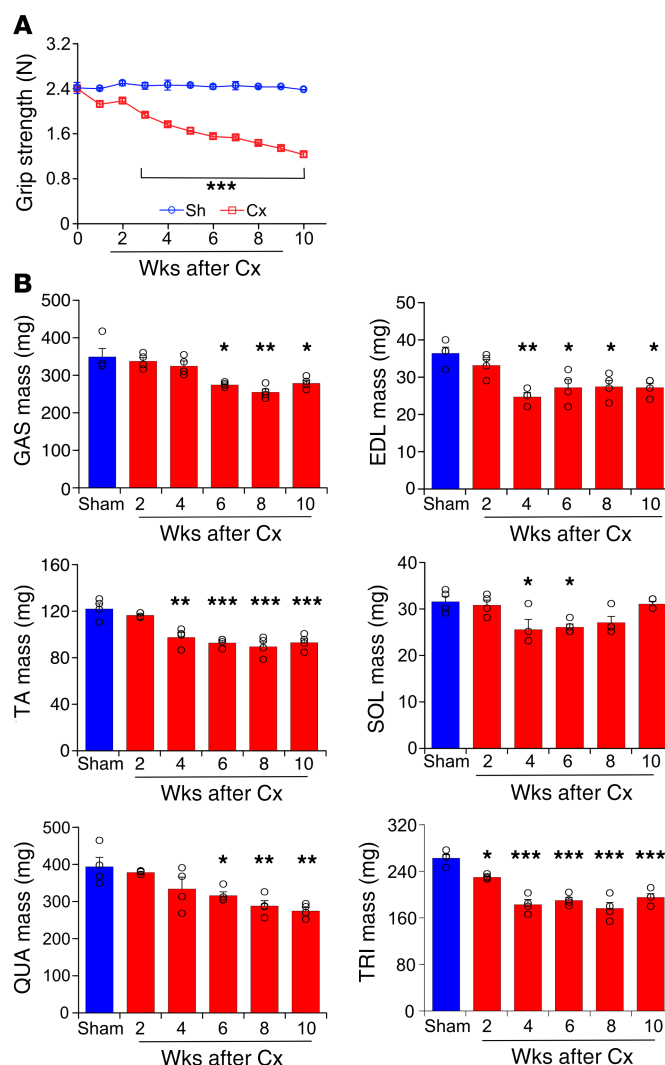


Figure 2. Strength declined coincident with loss of skeletal muscle mass after castration in mice bearing size-matched prostate tumors. (A) Adult PB-Cre4 *Pten*^{fl/fl} mice (starting volume $690 \pm 70 \text{ mm}^3$) were castrated (red, $n = 20$), or sham-castrated (Sh, blue, $n = 4$) and assessed weekly for grip strength, in newtons. The castrated mice were sacrificed in groups of 4 animals every 2 weeks after castration for tissue analysis. (B) Dissected skeletal muscle mass from each mouse, indicated by open circles. Columns are means; bars are SEM. * $P < 0.05$, ** $P < 0.01$, and *** $P < 0.001$ versus sham-castrated group determined using 1-way ANOVA with Dunnett's test.

Pan-myokine blockade prevents castration-induced sarcopenia in tumor-bearing mice. We next tested whether catabolic TGF- β family myokines are required for castration-induced sarcopenia in tumor-bearing mice. ActRIIB-Fc is a TGF- β family myokine ligand trap that specifically binds to and inhibits myostatin, the activins, GDF11, BMP9, and BMP10 (34). Administration of ActRIIB-Fc prevented the castration-induced loss of grip strength (Figure 4A, green versus red). Castration-induced skeletal muscle loss (Figure 4B) and lean body mass loss (Figure 4C) were also blocked by ActRIIB-Fc administration. In contrast, despite increased total body mass, mass of most skeletal muscles, and lean body mass in ActRIIB-Fc-treated versus vehicle-treated sham-castrated animals, strength was not increased by ActRIIB-Fc treatment in the sham-castrated mice (Supplemental Figure 7). Taken together, these data indicate one or more of the TGF- β family myokines mediates castration-induced sarcopenia.

GDF11 blockade prevents castration-induced strength loss in tumor-bearing mice. GDF11 was increased in muscle soon after castration, exclusively in tumor-bearing mice. Therefore, we tested whether GDF11 was required for castration-induced sarcopenia using a highly specific (Supplemental Figure 8), function-neutralizing (35), anti-GDF11 monoclonal antibody. From 3 to 5 weeks after castration, anti-GDF11 treatment of tumor-bearing mice slowed grip strength loss (Figure 4A, light purple line). At week 6 and later, anti-GDF11 treatment completely blocked the castration-induced grip strength loss (Figure 4A). GDF11 neutralization did not change the total body mass of castrated mice (Supplemental Figure 7B). Surprisingly, GDF11 neutralization did not reverse the castration-induced skeletal muscle mass loss (Figure 4B) or lean body mass loss (Figure 4C). These latter data indicate that although GDF11 largely mediates castration-induced strength loss, GDF11 neutralization is not sufficient to preserve muscle mass.

Castration-induced sarcopenia is exacerbated in tumor-bearing mice. We showed that in tumor-free mice, grip strength did not decline until 6 weeks after castration (16). In contrast, tumor-bearing mice demonstrated reduced grip strength within 3 weeks after castration in 2 tumor size-matched cohorts (cohort 2, Figure 2A, and cohort 3, Figure 4A). An earlier onset of strength loss was also observed in cohort 1, which consists of mice bearing a wider range of tumor volumes (Figure 1A). These data strongly imply that the presence of a tumor accelerated strength loss (Table 1, Onset column). Moreover, the magnitude of strength loss observed was about 50% greater in tumor-bearing mice (Table 1, Max loss column). Finally, the maximum degree of skeletal muscle mass loss (~20%) was reached by 4 weeks after castration in tumor-bearing mice, versus 10 weeks in tumor-free mice (Table 1). The accelerated strength and muscle mass loss is consistent with the earlier increases in catabolic TGF- β family myokines that we observed in tumor-bearing mice (Figure 3).

Castration induces GDF11 and myostatin in prostate tumors and in the circulation. Based on the accelerated sarcopenia and differences in muscle levels of catabolic TGF- β family myokine expression between tumor-bearing and tumor-free, myokine protein levels were measured in tumors and serum of serially sacrificed mice (cohort 2, Figure 2 and Figure 3). In tumor tissue, GDF11 was increased 2 weeks after castration (Figure 5A). This change paralleled the early increase of GDF11 levels in muscle (Figure 3, F and L) that occurred before strength loss. Myostatin levels were increased 8 and 10 weeks after castration in tumor tissue (Figure 5, B and C), well after the onset of strength loss. Activin (A, B, and AB) levels showed a mixed pattern of regulation in tumor tissue (Supplemental Figure 9). None of the mRNAs encoding the TGF- β family myokines, their receptors, or the muscle ubiquitin ligases was regulated in tumor tissue after castration (Supplemental Figure 10). Unexpectedly, while levels of circulating TGF- β family myokines did not change after castration in tumor-free mice (16), serum GDF11 was increased 2 weeks after castration in tumor-bearing mice (Figure 5D), at the same time we observed increases in tumor and muscle. Also in contrast to tumor-free mice, serum myostatin was increased both at 2 weeks and at 6 through 10 weeks after castration (Figure 5, E and F). Circulating activin (AA, BB, AB) levels were unchanged or undetectable and did not reflect the mixed pattern observed in tumor tissue (Supplemental Figure 9). Circulating levels of both GDF11 and myostatin were higher in animals bearing larger tumors (Supplemental Figure 11). We also assessed relative expression differences between muscle and tumor tissues. GDF11 protein levels were comparable between muscle and tumor (Figure 5G). However, myostatin was more than 10-fold higher in tumor than in muscle from both sham-castrated and 8-week-castrated animals (Figure 5, H and I). Taken together, these data suggest that the tumor is a possible source of endocrine TGF- β family myokines mediating sarcopenia.

Discussion

In this report we examined an autochthonous PrCa (PB-Cre4 *Pten*^{fl/fl}) mouse model for castration-induced sarcopenia to better understand the mechanism of ADT-induced sarcopenia in patients with PrCa. This model faithfully recapitulates human prostate cancers in a number of important ways. First, prostate-specific PTEN loss is a genetic lesion seen frequently in primary PrCa in patients (28). Second, in this model, PrCa tumors progress slowly enough to allow the manifestation of ADT side effects. Third, castration of tumor-bearing mice resulted in strength and skeletal muscle loss accompanied by fat gain (Figure 1 and Figure 2), very similar to the obese frailty syndrome observed in men with PrCa receiving ADT (11). Because there are no effective pharmacologic interventions for PrCa patients with ADT-induced sarcopenia (2, 5, 36), insights from our mechanistic studies in mouse models may facilitate the development of new treatments. Finally, this model shows no evidence of cancer cachexia. Specifically, there is no loss of total body mass or grip strength with increased tumor volume (Supplemental Figure 2). This eliminates the possibility that tumor cachexia effects are confounding our conclusions about ADT-induced sarcopenia.

Previously, we used the ActRIIB-Fc ligand trap to demonstrate that catabolic TGF- β family myokines are necessary for castration-induced sarcopenia in tumor-free mice (16). The myokines that induce sarcopenia are primarily muscle derived, and catabolic signaling is paracrine from muscle stem (satellite) cells to myofibers (37), with only a minor endocrine contribution (38). In tumor-free mice, myostatin, activin A, and activin AB levels are increased in skeletal muscle 2 to 4 weeks after castration, prior to the onset of strength and muscle loss that occurs 6 weeks after castration (16). Figure 4 shows that in PrCa tumor-bearing mice, myokines are similarly essential for the induction of castration-induced sarcopenia, as demonstrated by the effectiveness of ActRIIB-Fc in blocking both strength and muscle mass loss.

Although catabolic TGF- β family myokine signaling is required for castration-induced sarcopenia

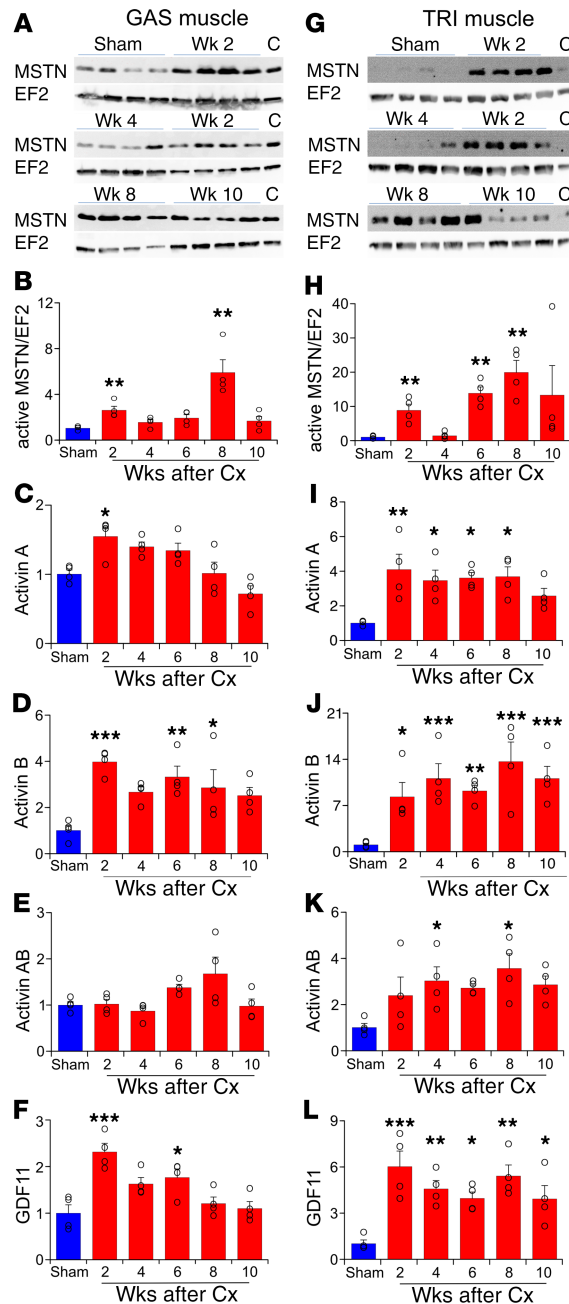


Figure 3. Castration increased active catabolic TGF- β family myokine proteins in skeletal muscles of tumor-bearing mice. (A–F) Protein expression in GAS muscle. **(A)** Representative immunoblots of soluble active myostatin (MSTN) C-terminal dimer and eukaryotic elongation factor 2 (EF2) expression in muscle from sets of 4 mice, castrated for the indicated times or sham castrated. Lanes of immunoblots marked “C” contain identical control sample for interblot comparison. **(B)** Quantification of relative MSTN levels for castrated mice (red) or sham-castrated mice (blue), from 3 determinations for each muscle (see Supplemental Figure 5 for additional immunoblots and supplemental materials for full, uncut gels). ELISA-determined protein levels of soluble active activin AA dimer **(C)**, activin BB dimer **(D)**, activin AB dimer **(E)**, and soluble GDF11 **(F)**, in muscle from 4 mice at each time point, measured 3 times each. **(G–L)** Protein expression in TRI muscle. **(G)** Representative immunoblot of MSTN and EF2 expression, as in **A**. **(H)** Quantification of MSTN levels, as in **B**. ELISA-determined protein levels of soluble active activin AA dimer **(I)**, activin BB dimer **(J)**, activin AB dimer **(K)**, and soluble GDF11 **(L)**, from 4 mice at each time point, measured 3 times each. Columns are sham-castrated normalized means at each time; bars are SEM. Individual mouse levels are indicated by open circles. * $P < 0.05$, ** $P < 0.01$, and *** $P < 0.001$ versus sham-castrated group determined using 1-way ANOVA and Bonferroni’s correction (**B** and **H**) or Dunnett’s test (**C–F** and **I–L**).

in both tumor-free and tumor-bearing mice, the kinetics of ADT-induced sarcopenia suggests that the presence of tumor influences muscle catabolism. The most striking differences were observed for muscle strength and mass changes (summarized in Table 1). When we compared cohorts of tumor-bearing mice with tumor-free mice, the tumor-bearing mice showed (a) an acceleration in the onset of castration-induced strength loss, (b) an increase in the magnitude of strength loss, and (c) a clear acceleration in the time to achieve maximal muscle mass loss. A second key difference is seen in the pattern of ADT-induced myokine levels in tumor-bearing versus tumor-free mice. For myostatin and the activins, the levels in the muscles of tumor-bearing mice at early time points after castration were similar to those of mice without tumors. In contrast, the level of GDF11 increased in the muscles of tumor-bearing mice, beginning 2 weeks after castration (Figure 3). GDF11 in muscle of tumor-free mice did not increase until 10 weeks after castration, well after strength loss (16). Unexpectedly, we also observed that GDF11 levels increased in both serum and tumor tissue 2 weeks after castration (Figure 5), suggesting that an endocrine mechanism might account for the corresponding increase of GDF11 protein in muscle. Specifically, we propose that castra-

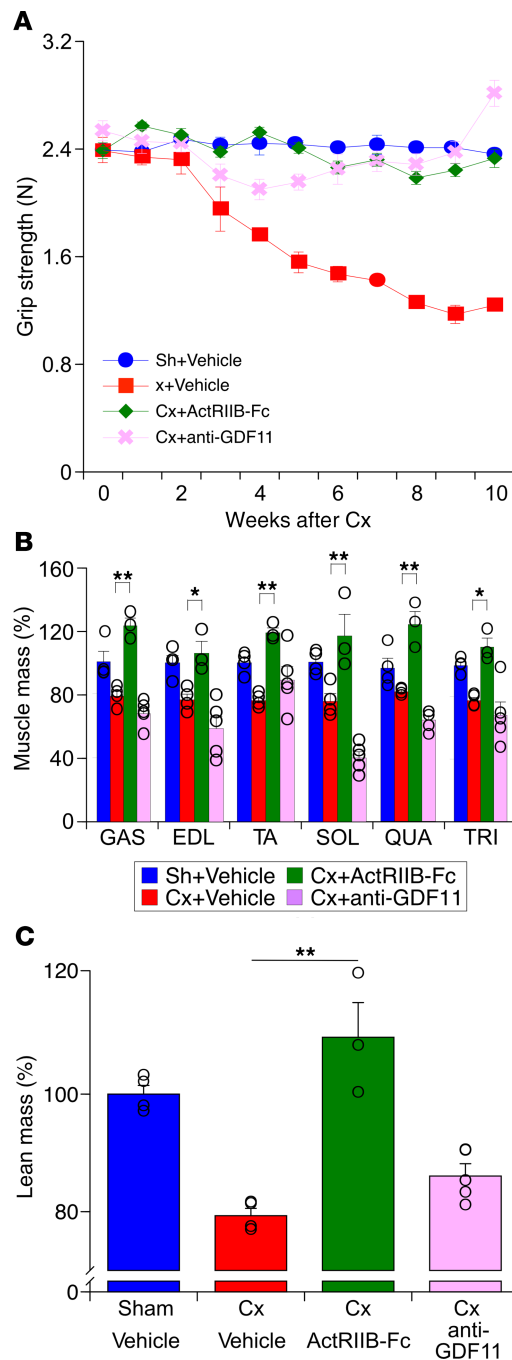


Figure 4. TGF- β family myokine ligand blockade reversed castration-induced sarcopenia. (A) Grip strength after castration or sham-castration of mice treated with PBS, ActRIIB-Fc, or anti-GDF11 antibody. (B) Dissected skeletal muscle mass 10 weeks after castration by dissection and weighing. (C) Lean body mass by quantitative NMR (qNMR), as percentage of sham-castrated mice. Mean indicated as lines or columns, SEM as bars; $n = 3\text{--}5/\text{group}$, indicated by open circles. * $P < 0.05$ and ** $P < 0.01$ for ActRIIB-Fc treated castrated versus vehicle-treated castrated mice determined using 2-way ANOVA and Tukey's honestly significant differences (HSD) test. See Supplemental Figure 7 for additional information.

tion induces GDF11 production in the prostate tumor, leading to elevated levels in the circulation and, subsequently, in muscle, where GDF11 acts by binding to ActRIIB to enhance muscle damage and strength loss (see model, Figure 6).

We believe that an endocrine mechanism is the most parsimonious explanation for GDF11 levels in the muscles of tumor-bearing mice. Alternatively, it is possible that a castration-induced increase in GDF11 protein levels in the muscles of tumor-bearing mice subsequently elevates GDF11 in the circulation and tumor tissue. However, our observations of the pattern of induction of another myokine — myostatin — argue against this alternative explanation. Specifically, we observed that myostatin was increased in both muscle and serum — but not in tumors — 2 weeks following castration of tumor-bearing mice (Figure 3 and Figure 5). This implies that elevated levels of muscle myokines can produce elevated serum levels but that tumor uptake of myokines from the serum is not efficient. It is noteworthy that at 8 weeks after castration, myostatin was increased in tumors, serum, and muscle, similar to the

Table 1. Tumor-bearing mice showed accelerated and more profound strength loss, along with accelerated muscle loss

Cohort	Strength loss		Muscle mass loss (%)				
	Onset (n)	Max loss (n)	2 wk	4 wk	6 wk	8 wk	10 wk
PrCa 1 ^A	4 wk (12)	41.3% (12)					17.4 ± 2.7 ^C
PrCa 2 ^A	3 wk (16)	48.8% (4)	5.9 ± 1.6	20.7 ± 3.8	22.6 ± 1.5	25.4 ± 2.5	21.1 ± 4.1
PrCa 3 ^A	3 wk (4)	49.6% (4)					21.9 ± 1.4
Tumor-free 1 ^B	6 wk (5)	40.2% (5)					24.7 ± 6.3
Tumor-free 2 ^B	6 wk (12)	31.7% (4)	6.6 ± 4.3	12.8 ± 3.3	13.1 ± 2.7	13.9 ± 2.8	18.9 ± 1.9
Tumor-free 3 ^A	6 wk (5)	28.8% (5)					21.4 ± 1.3

Castration-induced grip strength loss in 3 cohorts of PTEN prostate-KO tumor-bearing (PrCa) mice and 3 cohorts of the tumor-free parental C57BL/6 mice. Onset column shows earliest time after castration when strength loss was detected; max loss column shows maximum observed strength loss after castration, as a percentage of starting strength; and muscle mass loss column shows mean (± SEM) loss of mass of dissected muscles, as a percentage of the mass of muscles from sham-castrated mice, at the indicated time after castration. Tumor-free cohorts 1 and 2 were described in our previous report (16) and data further analyzed herein. ^AGrip strength measurements were performed weekly. ^BGrip strength measurements were performed every 2 weeks. ^CMuscle mass determined 16 weeks after castration.

pattern for GDF11 at 2 weeks after castration (see model, Figure 6). Finally, we also observed a correlation between tumor size and serum myostatin and serum GDF11 levels (Supplemental Figure 11). Overall, our results are most consistent with a unidirectional movement of GDF11 protein from tumor to circulation to muscle.

Regardless of the precise mechanism that produces an increase in GDF11 protein in the muscles of castrated tumor-bearing mice, treatment of these mice with an anti-GDF11 antibody blocked strength loss almost as efficiently as the ActRIIB-Fc ligand trap (Figure 4). Given the effectiveness of GDF11 blockade in our mouse model, we contend that tumor-derived GDF11 enhances the sarcopenic phenotype. Although GDF11 blockade reversed strength loss, it did not prevent muscle mass loss in castrated tumor-bearing mice (Figure 4). The failure to preserve muscle mass loss may be due to the high levels of circulating myostatin (Figure 5F) that appear to be derived from both muscle (Figure 3, B and H) and tumor (Figure 5C). The role of myostatin and the activins in castration-induced strength loss may be secondary, but their specific role in muscle catabolism and muscle quality relative to GDF11 may take on increased importance in countering ADT-induced sarcopenia in tumor-bearing animals.

Novel strategies are required to preserve strength and muscle mass for PrCa patients with ADT-induced sarcopenia, who may be at increased risk due to tumor endocrine signaling. Trials of pan-myokine blockade using ActRIIB-Fc were stopped because of bleeding complications, likely due to BMP9 neutralization (23, 24). Thus, rather than broad TGF- β family myokine blockade, specific therapy targets are needed to preserve muscle mass and strength for patients with sarcopenia. Blocking myostatin alone in patients with PrCa on ADT restored muscle mass but was not sufficient to reverse strength loss (39). Figure 4 demonstrates neutralizing GDF11 in PrCa-bearing mice preserved strength but not muscle mass. Whether preserving muscle mass is necessary to maintain function in men with PrCa treated with ADT for cancer control is unknown. If so, combining anti-GDF11 therapy with anti-myostatin (or anti-activin A) (40) therapy may prevent both strength and muscle mass loss, thereby improving patient quality of life.

Methods

PrCa model animals. Prostate-specific PTEN loss–induced PrCa-bearing mice (30) were produced by crossing male transgenic mice expressing probasin-driven Cre recombinase (PB-Cre4; obtained from the National Cancer Institute) with female floxed *Pten* mice (*Pten*^{LoxP/LoxP}; obtained from The Jackson Laboratory). The resulting PB-Cre4 *Pten*^{fl/fl} male pups were uniquely identified by implantation of a p-Chip (Pharmaseq) and genotyped for the Cre transgene and the *LoxP*-containing *Pten* alleles. All mice were maintained on a 12-hour light/12-hour dark cycle and had regular chow ad libitum. The probasin promoter is activated at puberty in prostate secretory epithelium to cause epithelial cell-specific deletion of *Pten*. Prostate adenocarcinomas form with complete penetrance between 3 and 7 months. Therefore, male PB-Cre4 *Pten*^{fl/fl} mice were monitored for tumor development using HFUS imaging

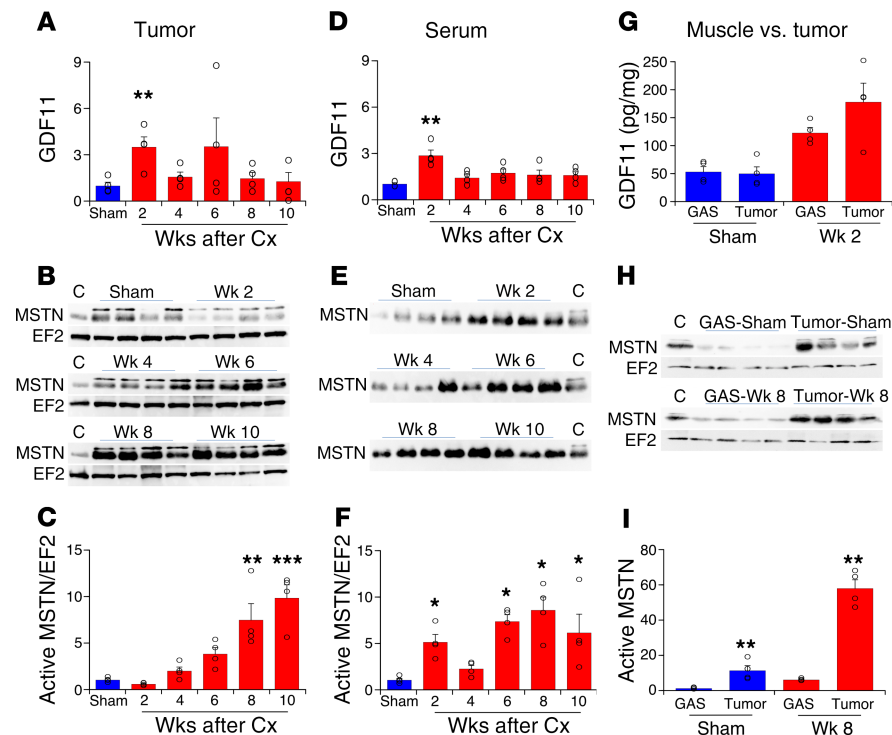


Figure 5. Castration increased GDF11 and myostatin in tumor and serum. (A–C) GDF11 and myostatin protein expression in tumor. (A) ELISA-determined levels of GDF11 in prostate tumor tissue, from 4 mice at each time, measured 3 times. (B) Representative immunoblots of soluble active myostatin C-terminal dimer (MSTN) and eukaryotic elongation factor 2 (EF2) expression in prostate tumor tissue from sets of 4 mice, castrated for the indicated times or sham castrated. Lanes of immunoblots marked “C” contain identical control sample for interblot comparison. (C) Quantification of MSTN levels in tumor tissue from castrated (red) or sham-castrated (blue) mice, from 3 determinations for each tumor (see Supplemental Figure 5 for additional immunoblots and supplemental materials for full, uncut gels). (D–F) GDF11 and myostatin protein expression in serum. (D) ELISA-determined levels of GDF11 in serum, from 4 mice at each time, measured 3 times. (E) Representative immunoblots of MSTN expression in equal quantities of serum protein from the 4 mice in A. (F) Quantification of MSTN levels in serum, as in B. (G–I) Comparison of GDF11 and myostatin protein expression between muscle and tumor. (G) ELISA-determined levels of GDF11 in GAS muscle and prostate tumor from sets of 4 mice, sham castrated (blue) or 2 weeks after castration (red), measured 3 times. (H) Representative immunoblots of MSTN in GAS muscle and prostate tumor from sets of 4 mice, sham-castrated or 8 weeks after castration. (I) Quantification of relative levels of MSTN between GAS muscle and prostate tumor. Columns are normalized means; bars are SEM. $n = 4/\text{group}$, indicated by open circles. $*P < 0.05$, $**P < 0.01$, and $***P < 0.001$ versus sham-castrated group (except G and I, GAS muscle vs. tumor tissue), determined using 1-way ANOVA and Dunnett’s test (A, D, and G) or 1-way ANOVA and Bonferroni’s correction (C, F, and I).

(see below) beginning at 12 weeks. Tumor-bearing animals were enrolled for experimental manipulation when the tumor was more than 300 mm³ and the animal was older than 6 months of age (adult). For cohorts 2 and 3, mice had tumors of 400–800 mm³ and were 6–9 months of age.

Mouse treatments, assessments, and tissues. Mice bearing a wide range of tumor volumes were castrated and monitored for 16 weeks as cohort 1. Subsequently, mice were assigned randomly to either sham-castrated or castrated groups to balance tumor volume in each group. Surgical castration was performed as previously described using isoflurane anesthetic (41). For ligand blockade experiments, castrated mice were assigned randomly to vehicle or ActRIIB-Fc (RAP-031, containing the murine Fc, Acceleron) treatment groups. ActRIIB-Fc administered twice weekly has maximal pharmacokinetic efficacy (42), and the homologous human ActRIIB-Fc has a half-life of 4 to 5 days in C57BL/6 mice after intraperitoneal injection (43). Mice were treated on the day of castration and subsequently twice weekly for 10 weeks with vehicle (Tris-buffered saline) or 10 mg/kg ActRIIB-Fc using intraperitoneal (IP) injection. GDF11 signaling was blocked using an anti-human GDF11 antibody (R&D Systems, Bio-Techne, MAB1958) that recognizes the GDF11 active dimer but not the closely related active dimer of GDF8 (myostatin, Supplemental Figure 8 and Supplemental Discussion) (35, 44, 45). Mice were treated with anti-GDF11 using a dose (100 µg administered IP twice weekly for 10 weeks) shown to neutralize GDF11 activity (40, 44, 46). Prostate volume was assessed using

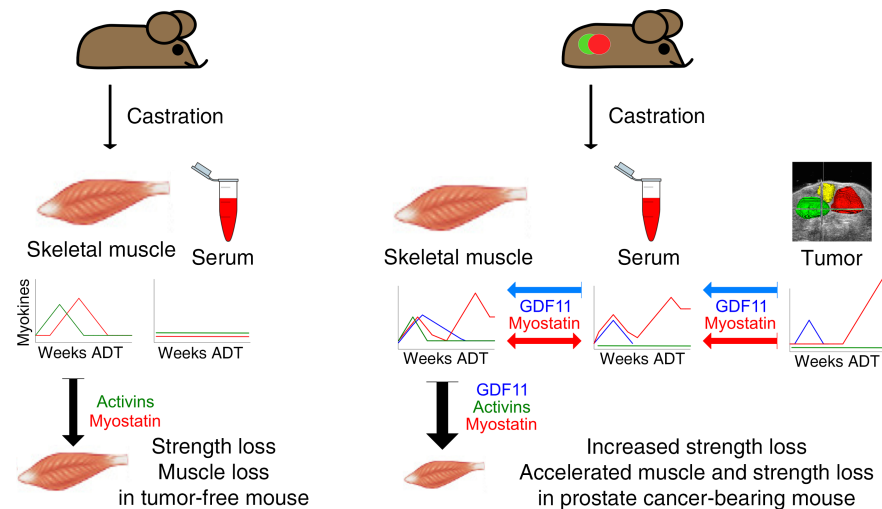


Figure 6. Model of ADT-induced catabolic TGF- β family myokine endocrine signaling in PrCa tumor-bearing mice.

Graphs of castration-induced changes in myokine concentrations (colored lines) in skeletal muscle and serum of mice without prostate cancer (left side) or in skeletal muscle, serum, and tumor of mice with prostate cancer (right side). Tumor lobes are represented by the green (left lobe) and red (right lobe) circles. In adult tumor-free mice myostatin and the activins increase after castration but prior to strength and muscle mass loss. In PrCa tumor-bearing mice, tumor secretes GDF11 (blue) and later myostatin (red) into serum. Endocrine-derived GDF11 and myostatin increase in muscle prior to strength loss (early myostatin also moves from muscle into serum). The tumor-derived catabolic TGF- β family myokines exacerbate castration-induced sarcopenia in tumor-bearing mice.

imaging at the indicated times, and grip strength and total body mass were measured weekly. Body composition was assessed using qNMR (LF-65, Bruker), and the mice were sacrificed at the prespecified endpoint. Calculations of whole-body lean mass excluded bone, fat, and fluid but included muscle, organ, tendons, ligament, and tumor. Consequently, mice bearing larger tumors had increased lean body mass because qNMR lean mass measurement includes tumor tissue (Supplemental Figure 3E), and therefore lean body mass is reported only for groups of mice that were tumor volume matched. Mice were anesthetized and blood was collected by cardiac puncture for serum myokine analysis. The tumor, hind limb, and forelimb skeletal muscles were dissected, weighed, snap-frozen in liquid nitrogen, and stored at -80°C until analysis.

Ultrasound imaging. We confirmed that our HFUS imaging protocol accurately measured prostate tumor growth in this autochthonous model with the same accuracy and low variability previously demonstrated for prostate orthotopic tumors (47). HFUS images of the prostate were acquired using a Vevo 2100 imaging system (Vevo LAZR; VisualSonics Inc.) equipped with a 21-MHz linear array transducer system (LZ250; 13- to 24-MHz maximal broadband frequency; 21-MHz center frequency, 75- μm axial resolution, 80- μm lateral resolution, 23-mm maximal lateral field of view). Briefly, mice were anesthetized, the abdomen was depilated, and B-mode images of the genitourinary area were acquired. 3D images of the prostate were reconstructed from 2D section images, and prostate volumes were computed using Amira 3D visualization software (FEI Visualization Sciences Group) (47). Tumors in each of the anterior lobes of the mouse prostate were visualized adjacent to the mouse bladder (Supplemental Figure 1A), and tumor volume increased as the mice aged (Supplemental Figure 1B). Tumor growth in a larger cohort of PB-Cre4 *Pten*^{fl/fl} mice was consistent up to 30 weeks of age (Supplemental Figure 1C). Initial tumor volume did not correlate with age after 6 months, but final tumor volume correlated with dissected tumor mass at sacrifice (data not shown and ref. 32). HFUS ensured biologic uniformity (i.e., similar tumor volume at the time of castration) and was used to confirm tumor regression after castration, demonstrating ADT was effective (Supplemental Figure 4). Imaging thus enabled comparison of the kinetics and extent of tumor regression to muscle mass and strength changes.

Physiologic measurements. Total body mass was measured using a digital balance (Ohaus), and 4-limb grip strength was assessed with a digital grip strength meter (Columbus Instruments). Briefly, mice were allowed to grab a horizontal wire grid attached to the meter using both forelimbs and hind limbs and then gently pulled by the tail until release. The mean maximum force (in newtons) of 3 consecutive trials with 3 minutes' rest between trials was taken as an index of grip strength. Mice were measured and assessed

before the start of experiments and were monitored weekly thereafter, in the morning of the same day of the week, in the same environment, by the same investigator, to minimize variability.

ELISAs. Tissue extracts were prepared by pulverizing dissected frozen gastrocnemius (GAS) or triceps (TRI) muscles or frozen tumor from individual mice using a pestle in a mortar containing liquid nitrogen, to obtain a fine powder. Frozen tissue powder was resuspended in NP-40 cell lysis buffer (30 mM Tris-HCl at pH 7.4, 150 mM sodium chloride, 1% NP-40, 1 mM sodium vanadate, 100 mM sodium fluoride, 2.5 μ M zinc chloride, 10% glycerol, 400 μ M phenylmethylsulfonyl fluoride, 1 \times protease inhibitor cocktail, MilliporeSigma) and sonicated for 8 seconds at 10 watts. Insoluble proteins were removed by high-speed centrifugation. The soluble supernatant was collected and stored at -80°C . Serum was isolated, diluted 1:1 with PBS, and stored at -80°C . Protein concentration was determined using bicinchoninic acid reagent (Pierce, Thermo Fisher Scientific). TGF- β family myokine dimeric protein levels were determined from equal amounts of total NP-40 cell lysis buffer soluble protein (or serum proteins) and total myostatin protein levels from equal amounts of acid-treated total soluble protein using ELISA according to the manufacturer's protocol. ELISA kits used were human/mouse/rat activin A ELISA kit (Quantikine DAC00B, R&D Systems, Bio-Techne), mouse activin B ELISA kit (E15932m, Cusabio Biotech Co., Ltd.), mouse activin AB and mouse GDF11 ELISA kits (CEA158Mu and SEC113Mu, respectively, Cloud-Clone Corp.), and total myostatin ELISA kit (Quantikine DGDF80, R&D Systems, Bio-Techne). ELISAs are non-cross-reactive versus other TGF- β family myokines (except activin A < 0.5% for activin AB); see Supplemental Discussion.

Immunoblot analysis. Active myostatin C-terminal dimer was measured using immunoblot because ELISAs do not discriminate this form from latent prodomain or inhibitor-bound myostatin C-terminal dimer (33). Equal amounts of soluble muscle tissue extract, tumor extract, or serum were separated on 10% SDS-PAGE under reducing conditions and transferred to nitrocellulose membranes. Membranes were bisected at a level corresponding to approximately 80 kDa. The lower membrane was incubated with rat anti-myostatin antibody (1:1000, clone 84214, R&D Systems, Bio-Techne MAB788), and the upper membrane was incubated with rabbit anti-EF2 antibody (1:2000, G270) (48), each diluted in 5% nonfat dried milk in Tris-buffered saline, overnight at 4°C and washed in Tris-buffered saline containing 0.1% Tween-20. The lower antimyostatin membrane was incubated in rabbit anti-rat IgG (1:20,000, Pierce, Thermo Fisher Scientific, 21218) for 2 hours at room temperature (RT), and both membranes were incubated in goat anti-rabbit horseradish peroxidase-conjugated antibody (1:20,000, Pierce, Thermo Fisher Scientific, 31460) for 2 hours at RT to detect the rabbit primary and bridging antibodies. Chemiluminescent (Supersignal West Pico, Pierce, Thermo Fisher Scientific) signal from the approximately 25 kDa active myostatin C-terminal dimer was captured using a cooled charge-coupled digital camera system (Kodak 4000R) and quantitated using Kodak Molecular Imaging software. Myostatin expression was normalized to EF2 expression levels from the same lane and then to an internal standard control on each gel/filter to allow comparison across different blots. Mean expression in each tissue from each animal was determined in triplicate. Inter-animal group means and standard errors were determined.

Statistics. Skeletal muscle mass, total body mass, grip strength, and ELISA TGF- β family myokine protein levels were compared using 1-way ANOVA and Dunnett's multiple-comparisons test for castration effects. Immunoblot quantifications of relative myostatin expression were analyzed using 1-way ANOVA incorporating a variance-stabilizing transformation and Bonferroni's correction for multiple-comparison analysis. Endpoint body composition changes were compared using 2-tailed Student's *t* test. Data were analyzed using 2-way ANOVA employing Tukey's HSD test to compare multiple therapy treatments' effects on grip strength, total body mass, lean body mass, and skeletal muscle mass. *P* values less than 0.05 were considered significant, and if reached, post hoc testing was performed. Statistical analyses were performed using JMP Pro 11.0 software (SAS) and R suite software.

Study approval. All animal studies were performed in accordance with the National Institutes of Health (NIH) *Guidelines for the Care and Use of Laboratory Animals* (National Academies Press, 2011) and approved by the Roswell Park Institutional Animal Care and Use Committee (1304M, 1308M).

Author contributions

JVC, JJK, and KLN conceived and designed the study. CP, SS, JVC, JJK, and KLN developed the methodology. CP, NJA, YZ, and SS performed the studies. CP, NJA, KHE, JJK, and KLN analyzed and interpreted the data. CP, NJA, SS, KS, JLM, KHE, JVC, JJK, and KLN wrote and revised the manuscript. The study was supervised by KLN and all authors approved the manuscript.

Acknowledgments

This work was supported by grants HHS-6-15SF and HHS-009-17SF from the SAS Foundation, 126771-IRG-14-194-11 from the American Cancer Society, a grant from the Roswell Park Alliance Foundation (to KLN), and NIH grants CA151753 (to JJK), S10OD010393-01, and P30CA016056. The funders had no role in study design, data collection and analysis, decision to publish, or preparation of the manuscript. We thank Richard Ngo for characterizing the anti-GDF11 antibody, Bruce Troen and Kenneth Seldeen for use of the qNMR instrument, and Scott Pearsall of Acceleron Pharma, Inc., for providing mouse ActRIIB-Fc (RAP-031). We thank the staff members of the Roswell Park Comprehensive Cancer Center's Cancer Center Support Grant-supported Experimental Tumor Models, Translational Imaging, and Laboratory Animal Shared Resource for their assistance.

Address correspondence to: Kent L. Nastiuk, Roswell Park Comprehensive Cancer Center, 665 Elm St., Buffalo, New York 14263, USA. Phone: 716.845.5771; Email: Kent.Nastiuk@RoswellPark.org.

1. Gilbert SM, Kuo YF, Shahinian VB. Prevalent and incident use of androgen deprivation therapy among men with prostate cancer in the United States. *Urol Oncol*. 2011;29(6):647–653.
2. Grossmann M, Zajac JD. Management of side effects of androgen deprivation therapy. *Endocrinol Metab Clin North Am*. 2011;40(3):655–71.
3. Sharifi N, Gulley JL, Dahut WL. Androgen deprivation therapy for prostate cancer. *JAMA*. 2005;294(2):238–244.
4. Afshar M, Evison F, James ND, Patel P. Shifting paradigms in the estimation of survival for castration-resistant prostate cancer: a tertiary academic center experience. *Urol Oncol*. 2015;33(8):338.e1–338.e7.
5. Nguyen PL, et al. Adverse effects of androgen deprivation therapy and strategies to mitigate them. *Eur Urol*. 2015;67(5):825–836.
6. Cruz-Jentoft AJ, Sayer AA. Sarcopenia. *Lancet*. 2019;393(10191):2636–2646.
7. Haseen F, Murray LJ, Cardwell CR, O'Sullivan JM, Cantwell MM. The effect of androgen deprivation therapy on body composition in men with prostate cancer: systematic review and meta-analysis. *J Cancer Surviv*. 2010;4(2):128–139.
8. Barbat-Artigas S, Pion CH, Leduc-Gaudet JP, Rolland Y, Aubertin-Leheudre M. Exploring the role of muscle mass, obesity, and age in the relationship between muscle quality and physical function. *J Am Med Dir Assoc*. 2014;15(4):303.e13–303.e20.
9. Cruz-Jentoft AJ, et al. Sarcopenia: revised European consensus on definition and diagnosis. *Age Ageing*. 2019;48(1):16–31.
10. Baracos VE, Martin L, Korc M, Guttridge DC, Fearon KCH. Cancer-associated cachexia. *Nat Rev Dis Primers*. 2018;4:17105.
11. Bylow K, et al. Falls and physical performance deficits in older patients with prostate cancer undergoing androgen deprivation therapy. *Urology*. 2008;72(2):422–427.
12. Bylow K, Hemmerich J, Mohile SG, Stadler WM, Sajid S, Dale W. Obese frailty, physical performance deficits, and falls in older men with biochemical recurrence of prostate cancer on androgen deprivation therapy: a case-control study. *Urology*. 2011;77(4):934–940.
13. Galvão DA, Taaffe DR, Spry N, Joseph D, Newton RU. Combined resistance and aerobic exercise program reverses muscle loss in men undergoing androgen suppression therapy for prostate cancer without bone metastases: a randomized controlled trial. *J Clin Oncol*. 2010;28(2):340–347.
14. Thorsen L, Nilsen TS, Raastad T, Courneya KS, Skovlund E, Fosså SD. A randomized controlled trial on the effectiveness of strength training on clinical and muscle cellular outcomes in patients with prostate cancer during androgen deprivation therapy: rationale and design. *BMC Cancer*. 2012;12:123.
15. Hanson ED, et al. Strength training induces muscle hypertrophy and functional gains in black prostate cancer patients despite androgen deprivation therapy. *J Gerontol A Biol Sci Med Sci*. 2013;68(4):490–498.
16. Pan C, Singh S, Sahasrabudhe DM, Chakkalakal JV, Krolewski JJ, Nastiuk KL. TGF- β superfamily members mediate androgen deprivation therapy-induced obese frailty in male mice. *Endocrinology*. 2016;157(11):4461–4472.
17. Klose A, et al. Castration induces satellite cell activation that contributes to skeletal muscle maintenance. *JCSM Rapid Commun*. 2018;1(1):e00040.
18. Lee SJ. Extracellular regulation of myostatin: a molecular rheostat for muscle mass. *Immunol Endocr Metab Agents Med Chem*. 2010;10:183–194.
19. Lee SJ, et al. Regulation of muscle growth by multiple ligands signaling through activin type II receptors. *Proc Natl Acad Sci U S A*. 2005;102(50):18117–18122.
20. Karsenty G, Olson EN. Bone and muscle endocrine functions: unexpected paradigms of inter-organ communication. *Cell*. 2016;164(6):1248–1256.
21. Le VQ, et al. Tolloid cleavage activates latent GDF8 by priming the pro-complex for dissociation. *EMBO J*. 2018;37(3):384–397.
22. Lee SJ, McPherron AC. Regulation of myostatin activity and muscle growth. *Proc Natl Acad Sci U S A*. 2001;98(16):9306–9311.
23. Attie KM, et al. A single ascending-dose study of muscle regulator ACE-031 in healthy volunteers. *Muscle Nerve*. 2013;47(3):416–423.
24. Smith RC, Lin BK. Myostatin inhibitors as therapies for muscle wasting associated with cancer and other disorders. *Curr Opin Support Palliat Care*. 2013;7(4):352–360.
25. Tao JJ, et al. First-in-human phase I study of the activin A inhibitor, STM 434, in patients with granulosa cell ovarian cancer and other advanced solid tumors. *Clin Cancer Res*. 2019;25(18):5458–5465.
26. Basaria S, Bhasin S. Targeting the skeletal muscle-metabolism axis in prostate-cancer therapy. *N Engl J Med*. 2012;367(10):965–967.
27. Ahima RS, Park HK. Connecting myokines and metabolism. *Endocrinol Metab (Seoul)*. 2015;30(3):235–245.
28. Armenia J, et al. The long tail of oncogenic drivers in prostate cancer. *Nat Genet*. 2018;50(5):645–651.

29. Barnett CM, et al. Genetic profiling to determine risk of relapse-free survival in high-risk localized prostate cancer. *Clin Cancer Res.* 2014;20(5):1306–1312.
30. Wang S, et al. Prostate-specific deletion of the murine Pten tumor suppressor gene leads to metastatic prostate cancer. *Cancer Cell.* 2003;4(3):209–221.
31. Mulholland DJ, et al. Cell autonomous role of PTEN in regulating castration-resistant prostate cancer growth. *Cancer Cell.* 2011;19(6):792–804.
32. Zhang W, et al. Inhibition of tumor growth progression by antiandrogens and mTOR inhibitor in a Pten-deficient mouse model of prostate cancer. *Cancer Res.* 2009;69(18):7466–7472.
33. Anderson SB, Goldberg AL, Whitman M. Identification of a novel pool of extracellular pro-myostatin in skeletal muscle. *J Biol Chem.* 2008;283(11):7027–7035.
34. Souza TA, et al. Proteomic identification and functional validation of activins and bone morphogenetic protein 11 as candidate novel muscle mass regulators. *Mol Endocrinol.* 2008;22(12):2689–2702.
35. Eggerman MA, et al. GDF11 increases with age and inhibits skeletal muscle regeneration. *Cell Metab.* 2015;22(1):164–174.
36. de Rooy C, Grossmann M, Zajac JD, Cheung AS. Targeting muscle signaling pathways to minimize adverse effects of androgen deprivation. *Endocr Relat Cancer.* 2016;23(1):R15–R26.
37. Parajuli P, et al. Twist1 activation in muscle progenitor cells causes muscle loss akin to cancer cachexia. *Dev Cell.* 2018;45(6):712–725.e6.
38. Lee YS, Huynh TV, Lee SJ. Paracrine and endocrine modes of myostatin action. *J Appl Physiol.* 2016;120(6):592–598.
39. Padhi D, Higano CS, Shore ND, Sieber P, Rasmussen E, Smith MR. Pharmacological inhibition of myostatin and changes in lean body mass and lower extremity muscle size in patients receiving androgen deprivation therapy for prostate cancer. *J Clin Endocrinol Metab.* 2014;99(10):E1967–E1975.
40. Latres E, et al. Activin A more prominently regulates muscle mass in primates than does GDF8. *Nat Commun.* 2017;8:15153.
41. Davis JS, Nastiuk KL, Krolewski JJ. TNF is necessary for castration-induced prostate regression, whereas TRAIL and FasL are dispensable. *Mol Endocrinol.* 2011;25(4):611–620.
42. Koncarevic A, et al. A soluble activin receptor type IIb prevents the effects of androgen deprivation on body composition and bone health. *Endocrinology.* 2010;151(9):4289–4300.
43. Chiu CS, et al. Increased muscle force production and bone mineral density in ActRIIB-Fc-treated mature rodents. *J Gerontol A Biol Sci Med Sci.* 2013;68(10):1181–1192.
44. Li H, et al. GDF11 attenuates development of type 2 diabetes via improvement of islet β -cell function and survival. *Diabetes.* 2017;66(7):1914–1927.
45. Zimmers TA, et al. Exogenous GDF11 induces cardiac and skeletal muscle dysfunction and wasting. *Basic Res Cardiol.* 2017;112(4):48.
46. Liu W, et al. GDF11 decreases bone mass by stimulating osteoclastogenesis and inhibiting osteoblast differentiation. *Nat Commun.* 2016;7:12794.
47. Singh S, et al. Quantitative volumetric imaging of normal, neoplastic and hyperplastic mouse prostate using ultrasound. *BMC Urol.* 2015;15:97.
48. Nastiuk KL, et al. FLICE-like inhibitory protein blocks transforming growth factor beta 1-induced caspase activation and apoptosis in prostate epithelial cells. *Mol Cancer Res.* 2008;6(2):231–242.